 doi:10.20944/preprints202009.0278.v1

Type of the Paper (Article)

A Study on The Influence of Chemical Nature of Fillers on Rheological and Fatigue Behaviour of Bitumen Emulsion Mastic

Ahmed Al-Mohammedawi[1,*], Konrad Mollenhauer[1]

[1] Engineering and Maintenance of Road Infrastructure, Transportation Institute, University of Kassel, Mönchebergstraße 7, 34125 Kassel, Germany.

* Correspondence: a.al-mohammedawi@uni-kassel.de

Abstract: Recently Cold Bitumen Emulsion (CBE) mixture technologies have been developed to lower the pavement construction temperatures to reduce the environmental costs and control the gas emissions. Due to its poor early mechanical strength, active fillers (i.e. cement) have been used to obtain high early stiffness in order to have the potential for timely construction of the next layer. There is, however, a lack of understanding about the impact of active fillers nature on viscoelastic behaviour and fatigue damage resistance of CBE mastics. This study, therefore, aims to identify the influence of active fillers on the rheological properties and the resulted fatigue behaviour of CBE mastic, supported by chemical analysis for the filler-bitumen emulsion. For this aim, bitumen emulsion was mixed separately with seven fillers/blended fillers to prepare the CBE mastics. Various experiments include continuous pH monitoring tests (chemical reactivity of filler-bitumen emulsion), Strain sweep (SS) tests, Temperature-Frequency Sweep (TFS) tests, Time Sweep (TS) tests, and Linear Amplitude Sweep (LAS) tests were conducted on the CBE binder and the prepared mastics. Results show that the rheological performance and the fatigue damage resistance is not only dependent on the filler inclusions, but it significantly relies on filler type and chemistry. Based on that, the raise in complex shear modulus and the decrease in viscous components were associated with a significant enhancement in fatigue performance for specific filler.

Keywords: Active filler; Bitumen emulsion mastic; Dynamic shear rheometer; Fatigue cracking resistance.

1. Introduction

The awareness of the sustainability and environmental issues in pavement construction has led to research being focused on the development of green asphalt pavement technologies, ultimately, aiming at a significant environmental, social, and economic benefit. Cold Bitumen Emulsion (CBE) mixture has several advantages over hot mix asphalt (HMA) in terms of conservation of natural material resources, reducing energy consumption, preservation of the environment, and reduction in cost. CBE mixture consists of an aggregate skeleton bonded by a thin-film material matrix (illustrated in Figure 1) composed of Bitumen Emulsion (BE) and mineral fillers [1], [2]. The mastic constitutes an essential part of the CBE mixture; consequently, its behaviour is highly governed by its mastic. The rheological response of the mastic is significantly controlled by the inclusion of fillers [3]–[5]. With this in mind, mineral fillers can be chemically categorized into active and inactive fillers based on their reactivity. Inactive fillers (i.e. basalt, limestone) are considered as inert fillers due to their chemical composition and generally used as a stiffness regulator by adding solid particles to the bitumen colloid system. However, there is no or little chemical reaction; hence the viscoelastic properties are maintained [6].

 doi:10.20944/preprints202009.0278.v1

Active fillers can be described as the fillers that react with water or with bitumen itself (changing bitumen structure) [7]. The most important chemical compounds in the active fillers that can control the mastic properties are CaO, and SiO_2. CaO gives fillers pozzolanic properties and, generally used to accelerate the setting time by forming $Ca(OH)_2$ as a hydration product [8]. The presence of SiO_2 tends to produce microstructures with low porosity and hence enhances the strength, but it inhibits the setting time [9]. The presence of CaO and SiO_2 together leads to the coexistence of the C-S-H phase with the geopolymer gel, which has been shown to improve the strength of the final product [10]. Moreover, adding Al_2O_3 to them leads to form the C-A-S-H phase, which provides the system with extra strength with short setting time [11]. Besides, some chemical elements have been found to have a negative effect on the cementitious binder such as Fe_2O_3, as this compound is found to hinder compressive strength [12]. Therefore, the filler should be carefully designed to achieve the desired rheological and mechanical properties, taking into account the mixture type (HMA or CBE).

CBE mastic behaviour and structure are different from that of HMA, as it comprises water in its system to have reduced viscosity for mixing and compaction. In CBE mixtures, the water needs to be evaporated to enable durable bitumen aggregate adhesion and high bearing capacity. In order to accelerate the curing process, active fillers are added to CBE mixtures. Consequently, water and active filler produce hydraulic binder, which can form rigid structures within the CBE mixtures. In this way, fillers improve the early mechanical properties but can lead to rigid long-term properties. Generally, fillers strengthen bitumen in three main mechanisms [13]–[15] particle geometry, volume filling, and chemical interaction. Particle geometry and volume filling are considered as mechanical reinforcement [15], [16]. Volume filling is caused by adding more solid particles to the system; therefore, high stiffness has resulted while chemical interaction includes the chemical composition and alkalinity of fillers. However, the response of CBE mastic modified with active filler may move from the viscoelastic range to pure elastic. Thus, CBE mastic could show low fatigue and fracture resistance under high load cycles [17]. Therefore, the mechanism of filler reinforcement of CBE mastic plays a major role in controlling the distresses and failure mechanisms in the CBE mixture [18].

During its service life, the CBE mixture is subjected to different distress. One of the most critical failures threatening CBE mixture can be fatigue cracking. This failure firstly appears as micro damages in the mastic and then, with increasing load cycles, grows up into macro cracks [19]. Thus, the physio-chemical and rheological characteristics of CBE mastic control the stress-strain distribution mechanism under thermal and traffic loading. In this research area, Anderson and Goetz (1973) conducted a study on using different fillers, and they concluded that different fillers have different reinforcing effects, depending on the nature of filler [20]. However, in an extensive study on dust collector fines, Anderson et al. (1982) came up with a conclusion that the nature and extent of the physio-chemical interaction need further studies [21]. Different methods have been tried by other researchers to study the physio-chemical interaction in terms of the effect of the chemical composition of fillers on mastics and/or asphaltic mixtures. Kandhal (1981) measured the pH values of a diluted water solution of fillers and stated that the pH values could hardly be related to how filler changes the mastic behaviour [22]. Recently, Ziyani et al. (2014) chemically investigated the reactivity of fine aggregate in bitumen emulsion by using the rise in pH test and element dissolution [23]. However, the physicochemical interaction between active fillers and bitumen emulsion and its effect on the rheological performance and fatigue damage resistance is not well investigated yet.

For bitumen emulsion, the physicochemical interaction starts at adding the destabilizing agent (filler) to the bitumen emulsion medium, initiating the breaking, and therefore, the coalescence is accelerated due to the increase in the salinity (pH increase). The increase in salinity occurs as a result of a decrease in the concentration of free H+ in the solution because of ionic exchange between H+ and alkali species from the mineral such as Ca++ (and also between the emulsifier molecules and the carbonate anion). The result of this reaction is a specific form of salt that can be absorbed by the interface region and improve adhesion property [24], [25]. This mechanism affects the bitumen-filler affinity in terms of controlling the contact angle, surface tension, adhesion work, and cohesion between bitumen and fillers, which in turn, could affect the cracks triggered by either adhesive failure at the filler-bitumen interface region or cohesive failure within the bitumen [26]. In this context,

Preprints (www.preprints.org) | NOT PEER-REVIEWED | Posted: 13 September 2020 doi:10.20944/preprints202009.0278.v1

incorporating fillers could either manage the crack failures within the mastic matrix or make CBE mastic, in some cases, very stiff (being very sensitive to fatigue cracking) [27], [28].

To characterize the fatigue damage resistance of mastic, various testing methods and approaches have been explored within the time fatigue sweep tests such as 50% reduction in the complex shear modulus [29], [30], the Drop in Phase Angle (DPA) [31], the Dissipated Energy Ratio (DER), the Ratio of Dissipated Energy Change (RDEC) [31], [32] and Energy Stiffness Ratio (ESR) [33], [34]. In different concept, Wen and Bahia (2009) developed a binder fatigue testing procedure based on an accelerate damage development in the specimen by means of applying a rapidly increased loading amplitude (strain). The raw data of this test is interpreted by the Viscoelastic Continuum Damage (VECD) mechanics theory principles, and then the fatigue law is obtained [35]. The critical review of state of the art shows that the studies dealing with the fatigue resistance are somewhat restricted to CBE mixture, knowing that the mastic being the actual binder in CBE mixtures. This research provides a comparative investigation on the chemical reactivity of active fillers and its consequences on the rheological properties and fatigue damage resistance of CBE mastics, employing Strain sweep (SS) tests, Frequency- Temperature sweep (FTS) tests, strain-controlled Time Sweep (TS) tests, Linear Amplitude Sweep (LAS) performed by Dynamic Shear Rheometer (DSR). Taking into consideration that each filler might influence the mastic fatigue-based properties in different fatigue-induced damage patterns.

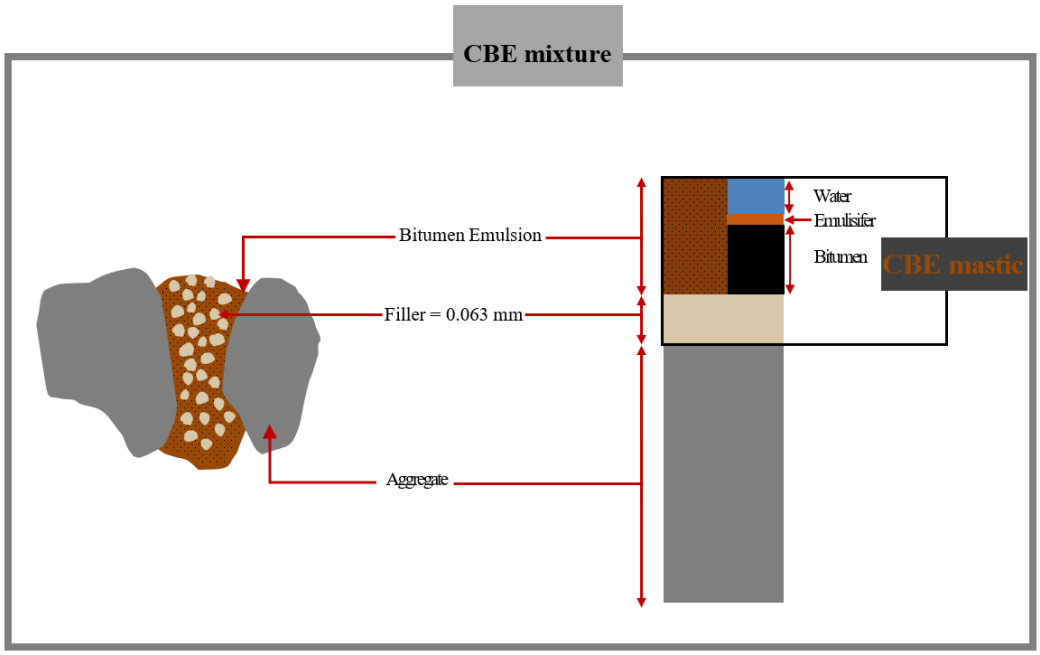

Figure 1. A schematic showing the CBE mixture components

2. Materials and Methods

2.1 Basic materials

Unmodified cationic bitumen emulsion type C60B10-BEM of penetration grade 70/100 was used to produce the BE specimens and to prepare all the mastics. In order to avoid the effect of the particle to particle contact, a relatively low mass ratio of 0.21 (filler to residual bitumen ratio lower than the practical ratio) was chosen. Thus, this ratio was expected to offer filler-CBE suspensions in diluted medium (low concentrated). In this regard, filler particles and the effective bitumen film around the filler particle, are dispersed and not expected to contact each other. The BE was mixed separately with limestone (LS), cement (CE), ladle slag (LD), silica fume (SF), ettringite (ET), geopolymer with an activator (GE) and geopolymer without activator (GO). ET blended filler was prepared by using 70% LD and 30% of Gypsum as recommended by Nguyen et al. [36]. GO blended filler was prepared

by mixing 55%LD, 35%Fly ash, and 10%SF. Then, GO was mixed with a 3.5% activator by its weight to prepare GE. The activator was a combination of 50% sodium hydroxide (NaOH) in the concentration of 10 M and 50% sodium silicate as an alkaline activator. All used filler particles are smaller than 63µm. The properties and chemical compositions of the fillers are given in Table 1.

Table 1. Properties and chemical composition (wt %) of used fillers.

Filler	SiO_2	Al_2O_3	CaO	SO_3	$CaCO_3$	Fe_2O_3	Other oxides (%)	Density (cm^3/g)	[1]Delta R&B
LS	0.53	0.16	0	0.08	98.03	0.08	1.12	2.73	1
CE	20.86	4.97	64.74	3.30	-	3.86	2.27	3.14	2.5
LD	8.33	28.91	52.41	1.83	-	1.39	7.13	2.58	1
SF	97.57	0.06	0.71	0.12	-	0.06	1.48	2.27	3
ET	6.29	20.30	49.18	18.02	-	1.02	5.18	2.62	2
GE	31.29	25.30	29.22	1.02	-	6.27	6.91	2.46	2
GO	31.29	25.30	29.22	1.02	-	6.27	6.91	2.46	2

[1]Mastics were prepared with hot bitumen (same grade) with the same bitumen to filler ratio.

2.2 Mastic preparation

In this study, a filler of 43 g was added and mixed gradually with 340 g of Cold Bitumen Emulsion (CBE) binder at 25°C, using a mechanical mixer. The mixing regime, as described in Figure 2a, was 5 min slow mixing (150 rpm) to initially agitate the filler into the CBE binder to help disperse the particles and then 500 rpm was applied continuously for 45 min. This mixing procedure was also performed to the CBE binder to avoid possible effects on results. During mixing, it was observed that there was no particle separation. However, at the end of mixing for certain fillers, breaking was noticed. In order to avoid the bubbles due to water evaporation, the mix was poured in a shallow glass dish. After 3 days of curing with 40°C and 65% RH, small specimens (approx. 8mm diameter) were cut for DSR testing, as shown in Figure 2b. DSR plates were heated up to 64°C, and then the specimens were carefully placed on the bottom plate. The upper plate was lowered to achieve 2 mm thickness. Afterwards, the unnecessary edges were trimmed.

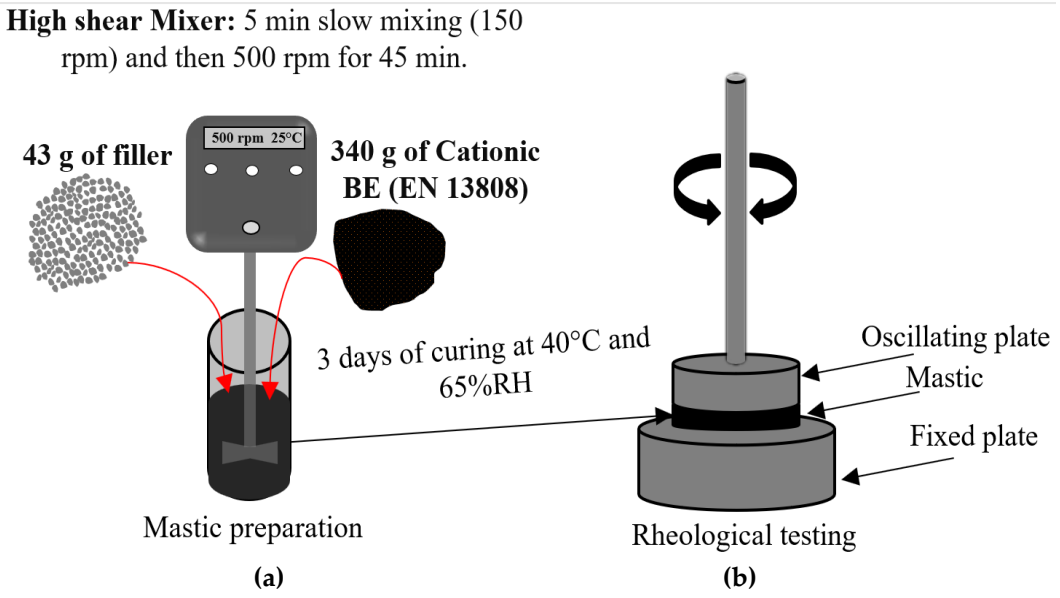

Figure 2. A schematic showing: **(a)** Mastic mixing and preparation; **(b)** DSR rheological testing

2.3 Experimental program

Preprints (www.preprints.org) | NOT PEER-REVIEWED | Posted: 13 September 2020 doi:10.20944/preprints202009.0278.v1

Various tests were performed using DSR, with an 8 mm parallel plate geometry and a 2 mm gap include SS, FTS, TS and LAS tests. Furthermore, continuous pH monitoring tests were performed using a pH meter. Each test is described in the following sections:

2.3.1. Strain Sweep (SS) test

SS tests were initially performed to determine the Linear Viscoelastic (LVE) limit and define a suitable range of deformation level. SS tests were conducted at -20°C, with a constant frequency of 10 Hz. From the results, a strain of 0.05% was found appropriate as per the LVE limit.

2.3.2 Frequency-Temperature sweep (FTS) test

The rheological properties of the CBE binder and mastics were characterized by FTS tests at a constant strain amplitude of 0.05% over a range of frequencies between 0.1 to 10 Hz and at temperatures from -20°C to 40°C. The resulted raw data was interpreted in the form of master curves [37], [38]. The master curves were constructed using the sigmoidal model Eq. (1) along with shift factor through horizontal Time-Temperature Superposition Principle (TTSP), following Arrhenius law Eq. (2) and Eq. (3) [39].

$$G* = G_0^* + \frac{G_\infty^*}{1 + e^{-\left(\frac{\ln fr - f_0}{z}\right)}} \quad (1)$$

$$\alpha_T = e^{\frac{-\triangle H}{R}\left(\frac{1}{T} - \frac{1}{T_{ref}}\right)}, \quad (2)$$

$$fr = \alpha_T * fi, \quad (3)$$

Where G^*, f_r, G_0^*, F_0, G_∞^*, z, α_T, R, $\triangle H$, T_{ref} and f_i are, respectively, the modelled complex shear modulus, the reduced frequency, the min limiting complex shear modulus, the min limiting frequency, the span of complex shear modulus value, the fitting parameter, the shift factor, the universal gas constant, the activation enthalpy for flow, the reference temperature (20°C) and testing frequency.

2.3.3 Time sweep (TS) test

A strain-controlled TS tests were carried out to assess the fatigue resistance of CBE mastics. The tests were conducted at 20°C temperature and 10 Hz of loading frequency with three different unique strain levels 1.5%, 2.5%, and 3.5%, which made fatigue failure in a reasonable time. Before the test, the testing duration is undetermined, and thus, in some cases, binders could take several hours to reach adequate damage in order to have a clear impression regarding their fatigue performance. Time sweep data for the tested CBE mastics were analyzed by five different approaches.

The first approach is the traditional fatigue definition. This approach is defined as the number of cycles to reach the 50% reduction in complex shear modulus ($G^*_{50\%}$). Figure 3 illustrates the number of cycles of a load to cause a 50% reduction in complex shear modulus versus other approaches. The second applied approach is the Drop in Phase Angle (DPA). DPA has been used commonly in the literature to identify the fatigue life. DPA and $G^*_{50\%}$ are plotted and shown in Figure 3a. It can be noticed that there is a sensible drop in phase angle after a steady increase. The drop in the phase angle indicates to the change in the proportion of complex modulus reduction.

The third approach is the Ratio of Dissipated Energy (DER). In the time sweep test, the Dissipated Energy (DE) per cycle can be obtained using Eq. (4) and therefore, the DER can be calculated using Eq. (5).

$$DE_i = \pi \varepsilon^2 G_i \sin \delta_i \quad (4)$$

$$DER = \frac{(\sum_{i=1}^{N} DE_i 0)}{DE_n} \quad (5)$$

Preprints (www.preprints.org) | NOT PEER-REVIEWED | Posted: 13 September 2020 doi:10.20944/preprints202009.0278.v1

where DE_i , ε, G_i , δ_i , $\sum_{i=1}^{N} DE_i$, and DE_n are, respectively, the dissipated energy at cycle i, the strain level, the complex modulus at cycle i, is the phase angle at cycle i, the accumulated dissipated energy up to cycle n, and the dissipated energy at cycle n. Figure 3b shows the DER plotted against the number of load cycles and compared with $G_{50\%}$ definition. The number of cycles to cause failure is the point on the curve at which the curve becomes nonlinear. Increasing load cycles results in steeper slope in the curve; thus, all the properties change very rapidly.

The fourth approach is the Ratio of Dissipated Energy Change (RDEC). The RDEC approach has been applied to eliminate the bias effects of dissipated energy (i.e. heat generation) and can be calculated using Eq. (7). RDEC has been suggested as a good indicator to define fatigue failure in bituminous materials RDEC [32].

$$RDEC = \frac{(DE_i - DE_{i+1})}{DE_i}, \tag{6}$$

where $RDEC$, DE_i and DE_{i+1} are, respectively, the ratio of the dissipated energy change per load cycle, the dissipated energy at the cycle i, and the dissipated energy cycle i + 1. In Figure 3c, RDEC values are plotted against the number of cycles and compared with $G_{50\%}$ criteria. From the plot, a plateau trend line can be noticed, which indicates that there is a constant quantity of energy turned into damage in the materials. The average of RDEC values in the plateau region is defined as plateau value (PV). The higher PV means, the higher energy amount is transformed to damage and consequently the lower fatigue life. The crack initiation can be identified when the REDEC values increase after the PV. This means that the material is damaged and no longer able to hold more cracks.

The last approach is the Energy Stiffness Ratio (ESR). ESR is a relatively new definition for fatigue life failure that has been developed by Mitchell et al. [33]; based on work done by Rowe and Bouldin [33]. ESR can be calculated as follows:

$$ESR = \left(\frac{G_i^*}{G_0^*}\right) * N_i, \tag{7}$$

where ESR, N_i, G_i^*, and G_0^* are the energy stiffness ratio, the number of cycles at i cycle, the complex modulus at the cycle i, and the initial complex modulus. Figure 3d shows the ESR values are plotted against the number of cycles and compared with $G_{50\%}$ criteria. The peak in the ESR curve indicates the number of cycles to cause fatigue failure. From the resulting plots of the failure criteria versus strain level, fatigue lives were evaluated. The fatigue was modelled by Eq. (8).

$$X_i = A.\varepsilon_i^B, \tag{8}$$

where X_i is the failure parameter, A and B are the fatigue coefficients and ε_i is the applied strain.

2.3.4 Linear Amplitude Sweep (LAS) test

LAS test is an accelerated fatigue test introduced recently [40], in which the strain level amplified systematically. The test starts firstly by identifying the undamaged linear viscoelastic properties of the specimens by conducting Frequency Sweep (FS). FS test was used with frequencies from 0.1 to 30 Hz under 0.05% strain level for 100 cycles. A relatively low strain level (0.05%) was used in this paper to ensure all mastics with the LVE limit. After that, the specimens were tested with Amplitude Sweep (AS) straight after the FS as no or little damage was expected during FS [41]. In the AS, the specimen was tested within a cyclic load, and the strain level amplified linearly from 0.1% to 30% under a 10 Hz frequency. LAS test was introduced as an accelerated fatigue test to reduce the testing time in comparison with the time sweep test [42]. The test results were analyzed using the VECD procedure to estimate the fatigue damage resistance. Schapery´s work potential theory (WPT) was used in the VECD approach to model fatigue damage growth [43]. Based on this theory, for a viscoelastic material (bituminous material), work can be correlated to damage by:

$$\frac{dD}{dt} = \left(-\frac{\partial W}{\partial D}\right)^{\alpha}, \tag{9}$$

Preprints (www.preprints.org) | NOT PEER-REVIEWED | Posted: 13 September 2020 doi:10.20944/preprints202009.0278.v1

$$\alpha = \frac{1}{1+m}, \tag{10}$$

where, W, D, α, and m are respectively, the work performed, the damage intensity, a material constant (the rate at which damage progresses) and the slope of a log-log plot of storage modulus (G') against to angular frequency (ω) that are derived from the first part of the test (frequency sweep test).

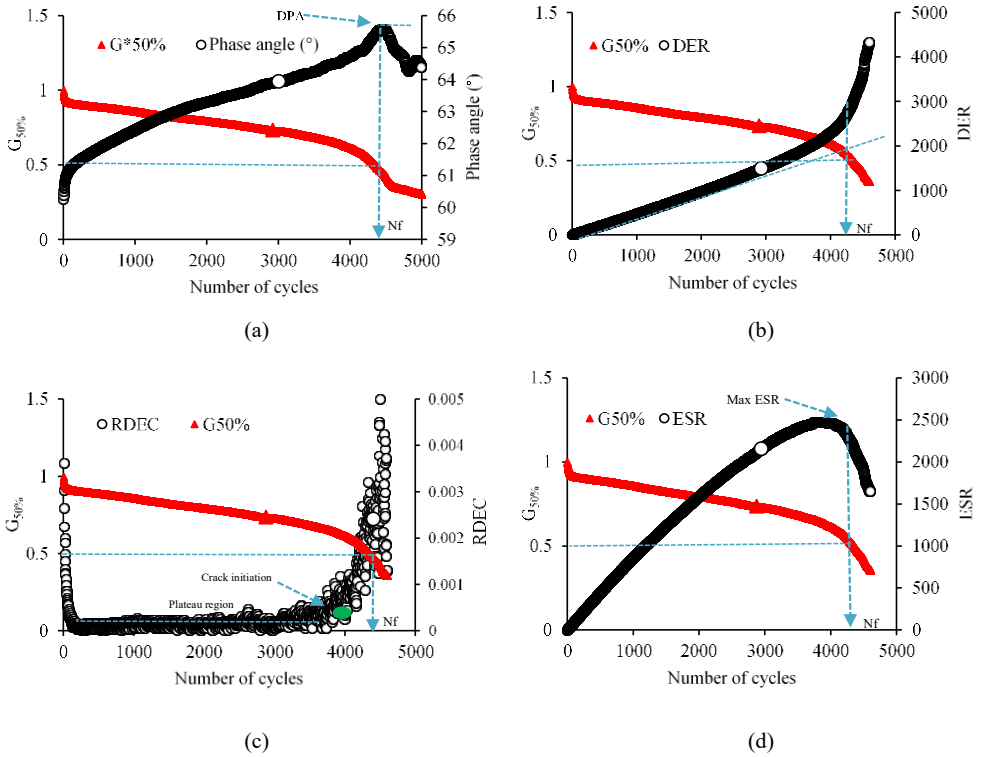

Figure 3. Comparing Nf for various approaches with the G50%: **(a)** DPA; **(b)** DER; **(c)** RDEC; **(d)** ESR

Based on Johnson (2010), the integrity parameter (C) and the accumulated damage (D) in the material due to the amplitude sweep (AS) loading can be predicted by using Eq. 11 and 12, respectively [41]:

$$\mathrm{C}(t) = \frac{G^* sin\,\delta}{G_i^*\, sin\,\delta_i}, \tag{11}$$

where $C(t)$, G^* and δ, G_i^* and δ_i and t are the integrity parameter, the complex shear modulus and phase angle at time t, the initial value of G* and δ, and testing time in seconds respectively.

$$D(t) = \sum_{i=1}^{N} [\pi * \gamma 0^2\,(C_{i-1} - C_i)]^{\frac{\alpha}{1+\alpha}} (t_i - t_{i-1})^{\frac{\alpha}{1+\alpha}}, \tag{12}$$

where, $D(t)$, $\gamma 0$, and t are the damage accumulation, the strain that is applied at a given data point (%) and is the test time (sec) respectively. The C(t) -D(t) relationship is established by the curve fitting technique using the power-law expression:

$$C(t) = C_0 - C_1[D(t)]^{C_2}, \tag{13}$$

where C_1 and C_2 are coefficients of fitting curve equations, whereas C_0 is the initial value of C(t). The fatigue law parameters A and B and then can be determined using the following expressions:

$$A = \frac{f(D_f)^{1+(1-C_2)\alpha}}{[1+(1-C_2)\alpha](\pi C_1 C_2)^{\alpha}}, \tag{14}$$

Preprints (www.preprints.org) | NOT PEER-REVIEWED | Posted: 13 September 2020 doi:10.20944/preprints202009.0278.v1

where f and D_f are the loading frequency (Hz) and the damage accumulation at failure, respectively. D_f can be defined as the damage accumulation (D(t)) value that makes a reduction of 35% in the integrity parameter (C(t)). In this study, 50% was used for comparison purposes. Df can be calculated:

$$D_f = \left(\frac{0.5}{C_1}\right)^{\frac{1}{C_2}}, \tag{15}$$

2.3.5 Chemical reactivity of filler-bitumen emulsion

The continuous pH monitoring tests were performed using HANNA HI5221 pH meter connected with pc for continuous monitoring, as shown in Figure 4. The testing procedure consists of adding 100 g of filler to 600 g of bitumen emulsion at 25°C temperature with a frequent stirring at a speed of 150 rpm. The monitoring of the pH value over time started for the bitumen emulsion for 10 minutes and then continued with filler addition to 2.7 hrs. The real-time measurements were recorded. Seven different fillers were tested separately in addition to the LS fillers, as reference filler.

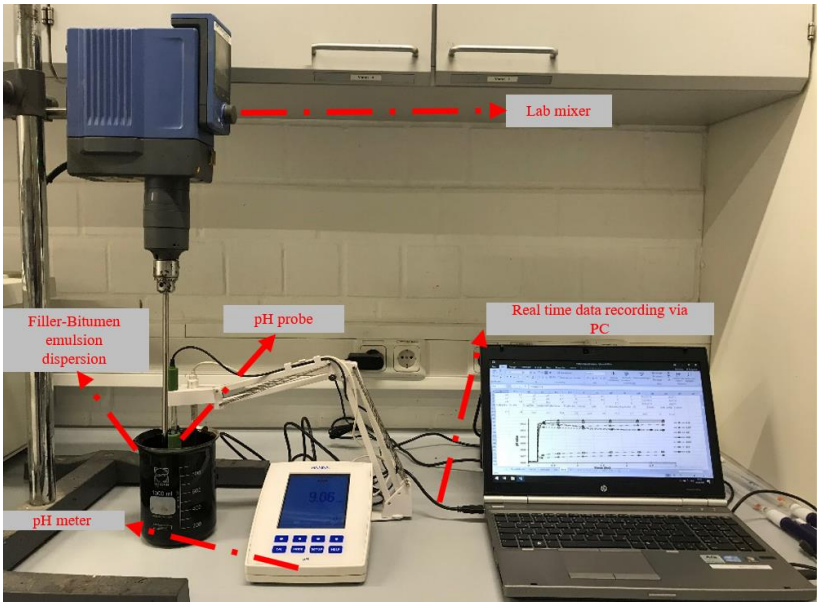

Figure 4. Experimental setup for continuous pH monitoring test

2.4. Goodness of fit

Four statistical approaches were performed to quantify the correlation of the measured and modelled data [44]–[46].

2.4.1 Standard error ratio

The standard error ratio is the ratio of the standard error of estimation (Se) and standard error of deviation (Sy). Se and Sy can be calculated using the following:

$$Se = \sqrt{\frac{\sum(Y - \hat{y})^2}{n - q}}, \tag{16}$$

$$Sy = \sqrt{\frac{\sum(Y - \tilde{y})^2}{n - 1}}, \tag{17}$$

where n is the sample size, q is the number model independent variables, Y is the measured complex shear modulus, $\hat{y}$ is the modelled complex shear modulus, and $\tilde{y}$ is the mean value of tested complex shear modulus. Smaller standard error ratio means perfect goodness of fit [47].

Preprints (www.preprints.org) | NOT PEER-REVIEWED | Posted: 13 September 2020 doi:10.20944/preprints202009.0278.v1

2.4.2 Coefficient of determination (R^2)

$$R^2 = 1 - \left(\frac{n-q}{n-1}\right) * \left(\frac{Se}{Sy}\right)^2, \quad (18)$$

$R^2 = 1$ indicates the perfect goodness of fit. The Se/Sy and R^2 standards are shown in Table 2.

Table 2. The goodness of fit statistics scale [47]

Criteria	R^2	Se/Sy
Excellent	⩾0.90	⩽0.35
Good	0.70–0.89	0.36–0.55
Fair	0.40–0.69	0.56–0.75
Poor	0.20–0.39	0.76–0.89
Very poor	⩽0.19	⩾0.90

2.4.3 The discrepancy ratio (*ri*)

$$ri = \frac{\hat{y}}{Y}, \quad (19)$$

where the subscript *i* refers to the data set number. *ri* = 1 refers to a perfect fit.

2.4.4 The Mean Normalized Error (MNE)

$$MNE = \left(\frac{100}{N}\right) * \sum_{i=1}^{N} \left(\frac{Y - \hat{y}}{\hat{y}}\right), \quad (20)$$

where *N* is the number of data, *MNE* = 0 indicates for a perfect fit.

3. Results and discussion

3.1 Chemical reactivity analysis of filler -bitumen emulsion

To provide a clear overview of alkaline effect and chemical composition of fillers on bitumen emulsion, the chemical reactivity of filler-bitumen emulsion in terms of the pH evolution is continuously monitored and plotted in Figure 5. Generally, all used fillers increase the pH of bitumen emulsion as a function of time. However, each filler has a different influence on bitumen emulsion, depending on its chemical composition. Thus, the SF and LS fillers raise the pH smoothly and slightly from 5.8 (bitumen emulsion pH level) to 7 and 6.5 respectively with a slight increase with time. This is due to their low ability to bind free H+ ions as both have low CaO content, and SF has high SiO_2 content. In contrast, due to their high CaO content and low SiO_2 content, GE, CE, LD, ET, and GO increased the pH dramatically to 12, 11.7, 11, 11.5, and 10.5 respectively. However, CE and GE fillers show a sudden increase in the pH value for the first few minutes until a constant pH value is reached. CE filler bonds most of the free H+ ions in the bitumen emulsion, forming C-S-H and C-A-S-H phase materials. These phases are known as stiff hydration products which offer extra strength to the mastics (detailed discussion in the next sections). While, the using of activator in GE filler increased the pH value to 12 because the pH of activator solution higher than that of the material itself, therefore, it activates the filler materials and then makes it able to bind more H+ ions. This observation can be clearly detected during the first few minutes when the pH increases smoothly as the fillers and activator are added to the bitumen emulsion. However, ET filler showed a completely different trend, as it showed a sharp increase in pH at the beginning because CaO reacts with water firstly and then exhibited a gradual decrease until it reaches a steady-state which is about 11 value. This trend is caused by the presence of Gypsum (neutral pH value) as it counterbalances the pH level of the solution, forming an ET binder.

Preprints (www.preprints.org) | NOT PEER-REVIEWED | Posted: 13 September 2020 doi:10.20944/preprints202009.0278.v1

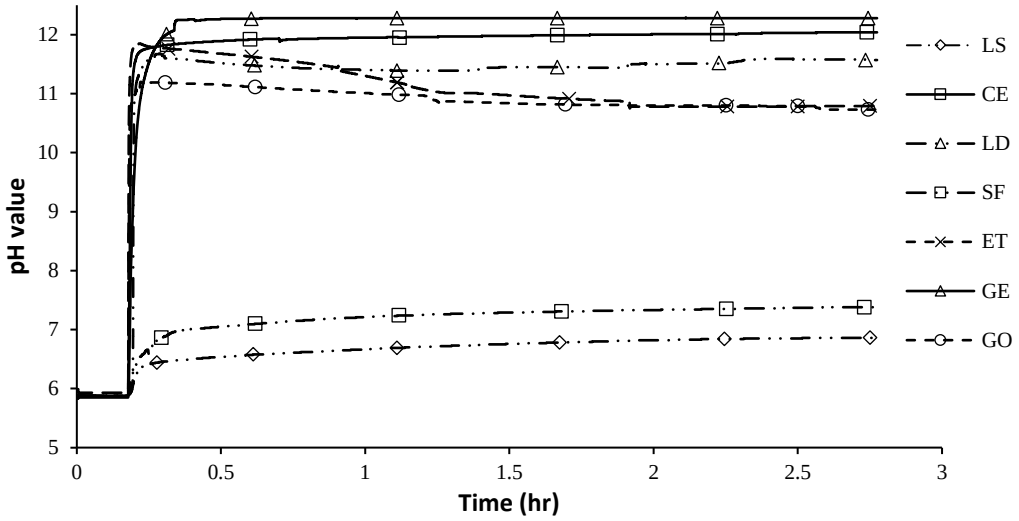

Figure 5. The chemical reactivity of filler-bitumen emulsion

Based on filler reactivity, a chemical analysis can be established hereby comparing the chemical composition of fillers with their pH value in bitumen emulsion. In this regard, only the silicon dioxide (SiO_2) and oxide calcium (CaO) oxides were considered related to the analysis. The other chemical compounds were not considered in this analysis. In addition, LS and GE fillers were not taken into account because LS is inert filler and does not have both earlier mention compounds while GE has the same GO chemical composition and pH is affected by the pH level of the activator. From Table 1 and Figure 5, linear correlations between pH change and CaO as well as between pH change and SiO_2 were established and plotted in Figure 6a and 6b, respectively. Figure 6a shows that the pH value increases as a function of CaO oxide. In this sense, the CaO content is noticeably higher for CE when it compared with other fillers, followed next by LD, ET, GE, GO, and SF fillers. As expected, the SF filler has the lowest pH value as it has shallow CaO content and high SiO_2 content.

In contrast, Figure 6b shows a different trend as the pH value decrease as a function of SiO_2 increase. These observations lead to the conclusion that there is a strong linear correlation between pH and filler chemical compounds contents (CaO and SiO_2). This remark explains why a particular filler has a specific pH level, which, in turn, has an effect on mastic rheological and fatigue behaviour.

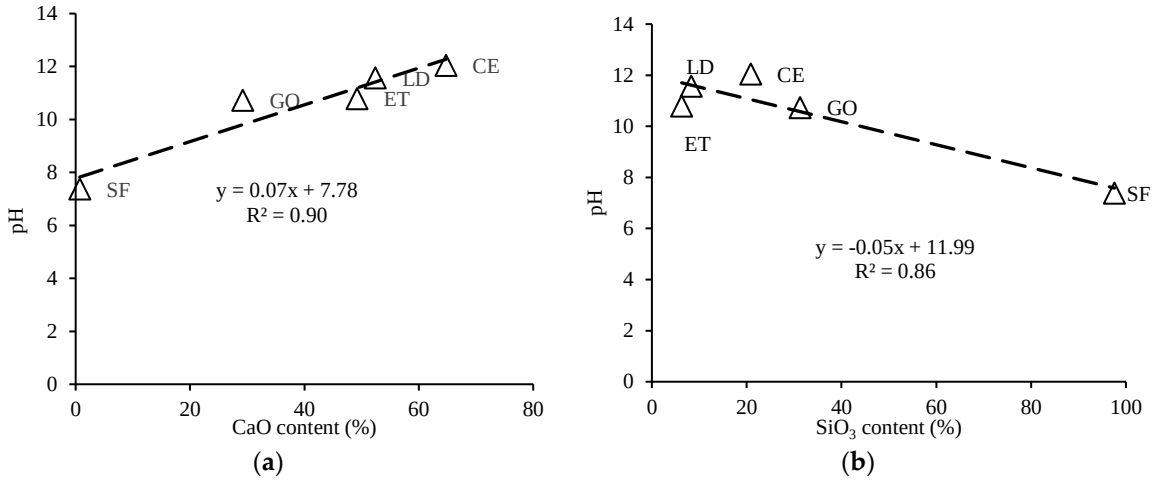

Figure 6. Correlation of pH of bitumen emulsion with: **(a)** CaO content%; **(b)** SiO_2 content%

3.2 Mastic rheological performance

3.2.1 Master curves

Preprints (www.preprints.org) | NOT PEER-REVIEWED | Posted: 13 September 2020 doi:10.20944/preprints202009.0278.v1

The complex shear modulus master curves were constructed using the shift factor equation based on the TTSP and modelled by the sigmoidal model are illustrated in Figure 7 and 8. For unobstructed view, the complex shear modulus and phase angle at 40°C and -20°C are stated in Table 3. From Figure 7 and 8, LS filler almost kept the complex shear modulus and the phase angle values the same as CBE binder at the whole range of frequencies. This effect could be due to adding an inert solid particle to the system; therefore, the viscoelastic property is maintained.

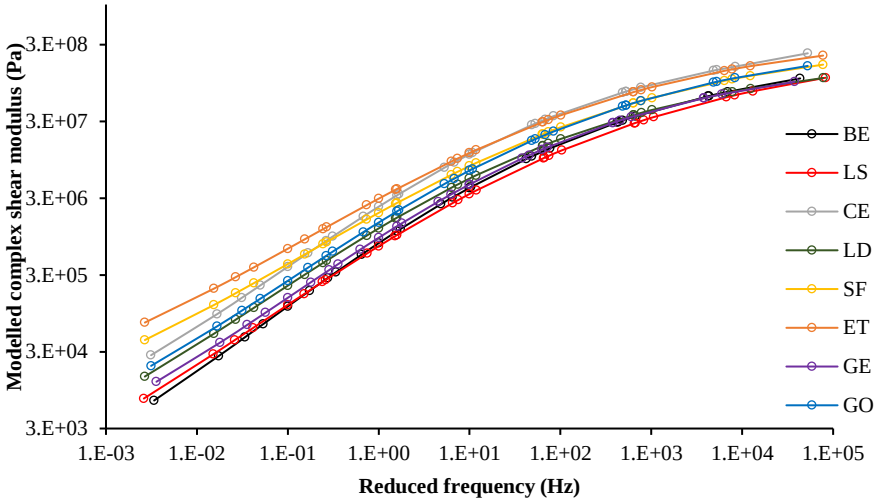

(**a**)

Figure 7. Modelled complex master curves of BE and CBE mastic at a reference temperature of 20°C

Furthermore, it is worth to note that GE and LD fillers have a similar effect on the CBE binder, both have higher complex modulus and lower phase angle at the whole range of frequencies compared to the CBE binder. The reason behind that is these fillers have the main compositions that form rigid phases (C-S-H and C-A-S-H) within the mastic. However, further investigations about the coexistence of these phases are required [48].

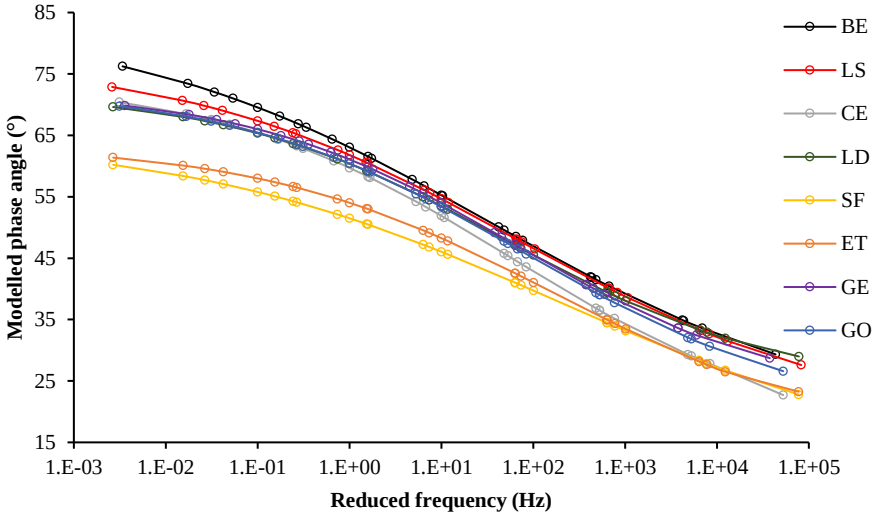

Figure 8. Modelled phase angle master curves of BE and CBE mastic at a reference temperature of 20°C

Using a geopolymer without activator (GO) shows higher complex shear modulus and lower phase angle than those of LD and GE at the whole range of frequencies, thus confer higher elastic

Preprints (www.preprints.org) | NOT PEER-REVIEWED | Posted: 13 September 2020 doi:10.20944/preprints202009.0278.v1

property on mastic (higher deformation resistance). As expected, CE mastic exhibited higher complex shear modulus and lower phase angle than those of GE, LD, and GO, especially at high frequencies. Despite having different chemical compositions, ET and SF have a relatively similar effect on BE. They showed the highest stiffening potential, and the lowest phase angle among all tested mastics over the whole frequency range. This observation, however, does not involve CE at high frequencies since it has the highest complex modulus in that zone. This inversion showed that CE mastic being stiffer than ET and SF. In this context, higher complex modulus and lower phase angle are not usually preferable at low temperatures as it makes the CBE mixture very stiff and very sensitive to cracks development. More information about crack resistance is described in the fatigue performance section.

Table 3. Complex shear modulus and phase angle at -20°C and 40°C

Mastic	Complex shear modulus (Pa)		Phase angle (°)	
	40°C	-20°C	40°C	-20°C
BE	6.957E+03	1.091E+08	76.24	29.33
LS	7.374E+03	1.113E+08	72.88	27.60
CE	2.707E+04	2.316E+08	70.41	22.00
LD	1.426E+04	1.104E+08	69.62	28.99
SF	4.265E+04	1.649E+08	60.21	22.79
ET	7.202E+04	2.163E+08	61.38	22.10
GE	1.221E+04	9.846E+07	69.84	28.72
GO	1.965E+04	1.587E+08	69.76	26.59

3.2.2 Statistical analysis

Figure 9 illustrates a graphical comparison between the measured and modelled data, which is considered a simple and easy visualized tool to identify the precision of modelling. In this graph, the measured and modelled values were equated and graphically represented.

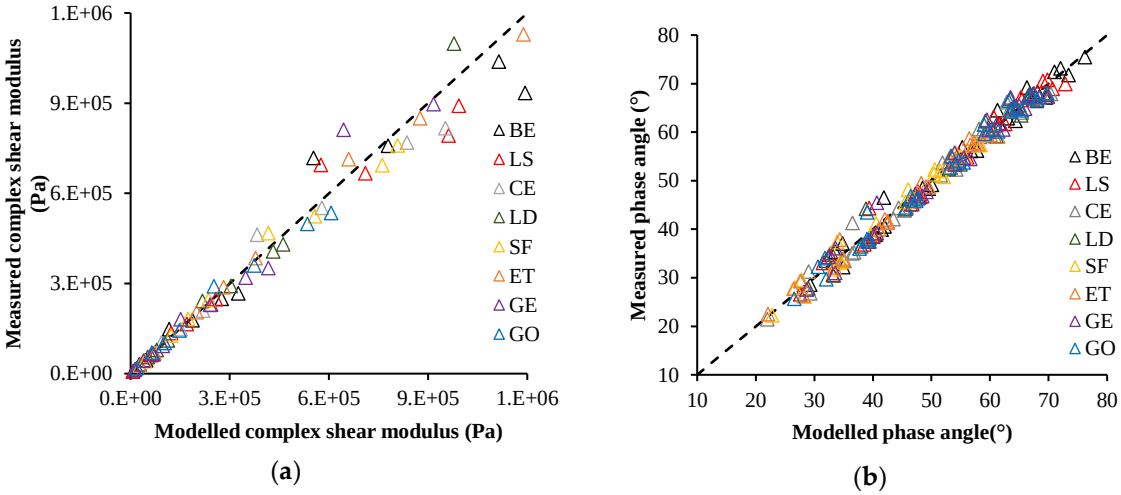

Figure 9. Graphical comparison between measured and modelled: **(a)** complex modulus data; **(b)** phase angles data.

From Figure 9a, it can be observed that the sigmoid model can describe complex shear modulus values for the BE and CBE mastics perfectly. However, the modelled complex shear modulus of all specimens slightly diverges from the equality line, particularly at lower temperatures (higher complex shear modulus values). On the other hand, Figure 9b shows a correlation between measured and modelled phase angle values. For all specimens, a good correlation between measured and modelled data was noticed. Besides, a statistical correlation between the measured and modelled

Preprints (www.preprints.org) | NOT PEER-REVIEWED | Posted: 13 September 2020 doi:10.20944/preprints202009.0278.v1

complex shear modulus and phase angle data were performed and are illustrated in Table 4a and 4b, respectively. In general, the R^2 and Se/Sy for all samples have excellent goodness of fit between the measured and modelled data. As expected, complex shear modulus data have higher correlations than the phase angle data. The ri method was employed to detect the tabularization of modelled data from the equality line. Therefore, a larger or smaller value for the ri (ri =1 for a perfect fit), it means that how much the modelled data is far from the measured data. All tested data were distributed around the equality line. Similar to the ri, the MNE was also applied to detect the correlation between measured and modelled data. All specimens showed a good correlation. However, the complex shear modulus data exhibited a better correlation than the phase angle. From Table 4a and 4b, it can be noticed that the ri is not consistent to observe the goodness of fit because there are only small variances between measured and modelled data. Consequently, R^2, Se/Sy, and MNE are suggested to identify the correlation between the modelled and measured data.

Table 4. Statistical analysis for master curves: **(a)** the complex modulus; **(b)** phase angle.

Sample	(a)				(b)			
	R^2	Se/Sy	MNE	ri	R^2	Se/Sy	MNE	ri
BE	0.996	0.066	0.892	1.000	0.982	0.147	3.015	1.000
LS	0.998	0.053	0.668	1.000	0.984	0.140	2.997	1.000
CE	0.997	0.059	0.682	1.000	0.983	0.143	3.506	1.000
LD	0.991	0.103	1.235	1.000	0.976	0.170	3.404	1.000
SF	0.997	0.059	0.649	1.000	0.986	0.131	2.693	1.000
ET	0.998	0.044	0.433	1.000	0.988	0.122	2.596	1.000
GE	0.996	0.066	0.770	1.000	0.977	0.167	3.337	1.000
GO	0.997	0.056	0.649	1.000	0.983	0.143	3.039	1.000

3.3 Fatigue performance

3.3.1 Time sweep test

In this paper, all CBE mastics were tested with a controlled strain time sweep test at a frequency of 10 Hz that is traditionally utilized in time sweep fatigue tests and under 20°C temperature. According to the fatigue definitions previously mentioned, the fatigue laws and lives of all tested mastics were evaluated from the fatigue approaches and are summarized in Figure 14 and Table 5, respectively. According to the achieved results, it can be observed that the different mastics have different fatigue coefficients and, therefore, reached different numbers of load application to show failure and all mastics (except LS mastic) have fatigue resistance greater than that of the CBE binder. LS and ET corresponding mastics have the lowest and the highest fatigue life respectively compared with the rest of mastics. Therefore, the fatigue life of tested mastics can be ranked as follows: ET > Go & GE > SF > CE > BE > LS.

3.3.2 LAS Results Analysis

The LAS test comprises two steps FS and AS. Firstly, FS test was carried out before the AS test in order to evaluate the undamaged behaviour of the specimen. With FS, a strain of 0.05% was applied under frequencies starting from 0.1 to 30 Hz. Small strain level was used to guarantee that the specimens are within the linear viscoelastic limit. Afterwards, from storage modulus (G') and angular frequency (ω) data, a log-log scale plot is derived. Then, the reciprocal value of the slope (m) of the linear regression model is calculated. Secondly, a linear AS was performed from 0.1 to 30% under 10 Hz frequency. Therefore, the parameters C_1 and C_2 are determined from the damage characteristic curve (C × D). Finally, the fatigue coefficients (A and B) and laws are then calculated from Eq. (9).

The complex shear modulus and the phase angle over the tested frequency range resulted from the frequency sweep test of the LAS testing procedure at the testing temperature of 20 C are graphed in Figure 10. The complex shear modulus raised as frequency increased. It can be observed that the

Preprints (www.preprints.org) | NOT PEER-REVIEWED | Posted: 13 September 2020 doi:10.20944/preprints202009.0278.v1

CBE binder has the lowest complex shear modulus when it compared with the mastics. However, LS mastic almost has complex shear modulus value similar to that of BE. It is interesting to notice that at lower frequencies, the viscous part of CBE binder is higher than that of mastics; consequently, it has additional time to relaxed than at higher frequency region. This is due to the fact that the filler incorporation increases the elastic part and decreases the viscous part. Nevertheless, due to the shortage of time, the difference is less noticeable as the frequencies increase. In general, the results of FS are quite similar to the master curves results in Figure 7 and 8.

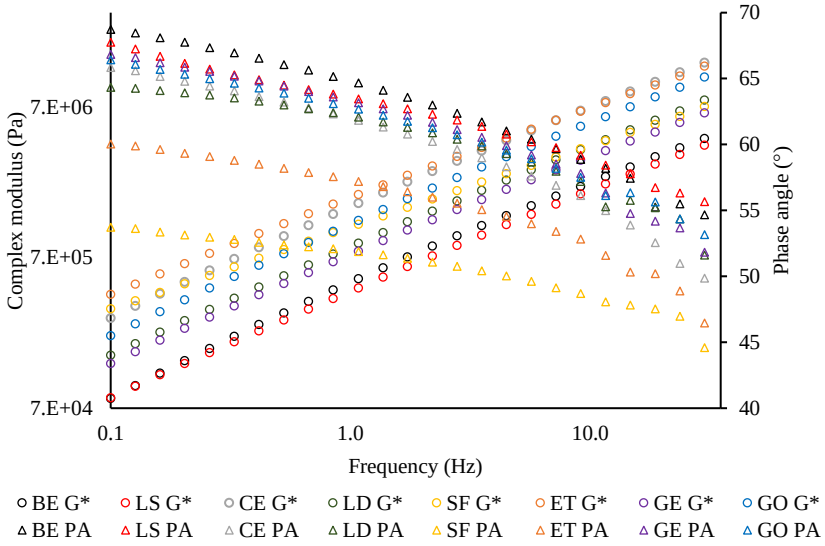

Figure 10. Master curves from frequency sweep of LAS test at 20°C for CBE binder and mastics

Figure 11 shows the stress-strain relationship for the tested specimens. Three regions were characterized and used to identify the fatigue failure from the stress-strain curve: the strain value at the peak, the plateau value of the peak, the steepness of curve (before and after the peak). In the initial part of the curve, the shear stress increases linearly as the strain increased. An additional increase in the strain amplitude decelerates the growth of the shear stress. This is the point at which the specimens start behaving in nonlinear trend as it gets in the nonlinear zone. Mastics approach the peak of the shear stress at various strain levels. After the peak zone, the shear stress drops down as the strain amplitude increases, imparting substantial damage has been produced in the specimen. Thus, a sharp decrease in this region means fast induced damage. Apparently, the peak stresses of the mastics are higher than the CBE binder. This behaviour is related to the mastics' higher complex shear modulus at 20 °C temperature, as previously depicted by the complex shear modulus master curves Figure 10 and explained in the stiffening index (Si) in Figure 12. From Figure 11 and 12, it can be observed that as Si decreases, the peak shear stress decreases because of the complex shear modulus reduction, which needs lesser stresses to deform the material.

However, not all mastics with high Si reach the peak of stress at a lower strain level (such as CE mastic). This indicates that carrying capacity before failure depends on filler type and interaction with the bitumen. Normally, greater complex shear modulus compels an increment in the stress level, and therefore the specimen bears a smaller amount of damage at failure (behave as fragile material). This effect is, nevertheless, filler type conditional. The addition of active filler to CBE binder alters the strain amplitude, where the peak of stress takes place. According to above, mastic with LS, as inactive filler, showed a sudden drop in shear stress after a relatively small plateau at 4.5% strain value, which was not seen for the rest of mastics, whereas without filler (CBE binder) the curve continues with smooth falling at 5% strain. As LAS test is an accelerated test, the used strain amplitudes exceed the viscoelastic region of mastics (and bitumen), and the strain dependence changes with the filler type. Therefore, the post-peak part of specific mastics shows discrepancies (nonlinear behaviour).

Preprints (www.preprints.org) | NOT PEER-REVIEWED | Posted: 13 September 2020 doi:10.20944/preprints202009.0278.v1

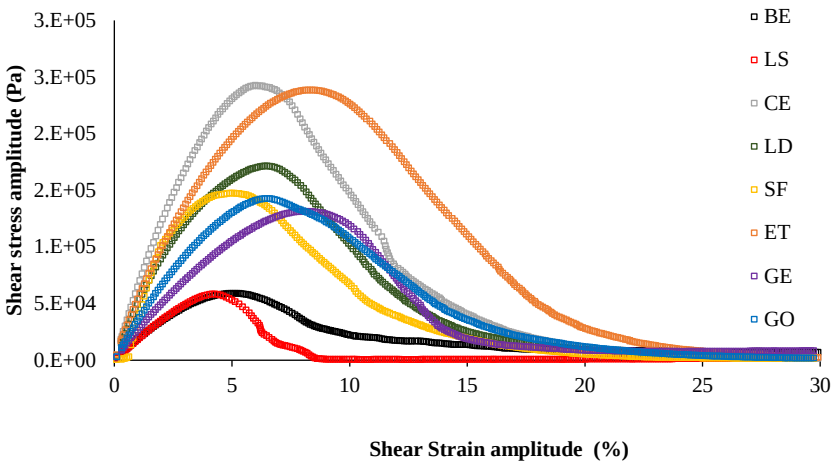

Figure 11. Shear stress-strain of different mastics

This can be clearly detected with LS mastic (and also for CE mastic). With SF filler, the mastic exhibited a sudden increase, with a short peak, and then it starts decreasing at 5% strain, indicating that it has low damage resistance. For CE mastic, the peak region was small, and there was a sudden reduction after the peak, starting at 6% strain. ET and GE have delayed the falling of the curves at 8% strain and have the mildest falling slope compared to other mastics, with an extended plateau region at peak zone. Mastic with LD filler showed stress peak curve shape similar to that of the CE corresponding mastic (at 6.5% strain) but with lower stress level. This could be due to the similar chemical composition.

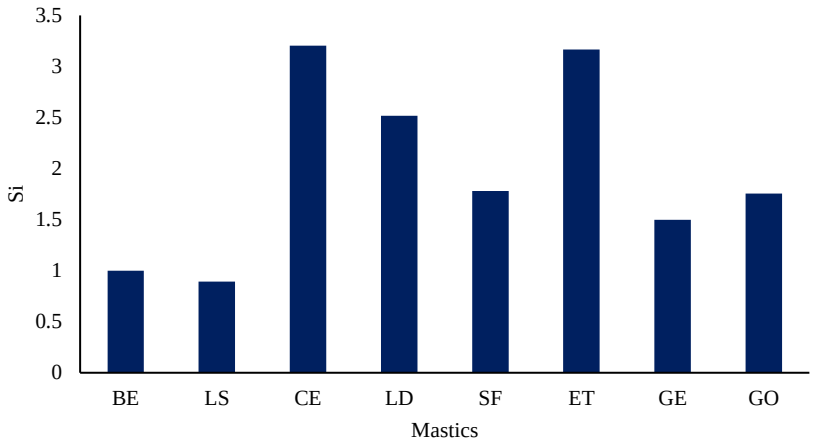

Figure 12. Stiffening index (Si) of different mastics at 20°

However, LD contains lower CaO content (less stiffening effect). Unlike the GE mastic, GO exhibited a very short plateau zone, and this difference could be attributed to the using of the chemical activator. Generally, the addition of active filler causes a phase inversion and forms a network of hydraulic binder within the mastic matrix. This binder conveys more considerable elasticity to the mastic and, accordingly, greater resistance to rutting deformation and could also offer good fatigue cracking resistance. For this reason, larger strain amplitudes are needed before the failure happens. These outcomes can be linked to the chemical reactivity of filler and its physicochemical interaction, as discussed in sections 3.1 and 3.4.

Figure 13 shows the damage characteristics (C- D) curves of the tested specimens. Generally, the C- D curves characterized by rapid growth at the initial strain amplitudes and then a segment of slight variation at the peak, ending with decreasing region, which is said to be associated to specimen degradation. The pattern of C-D curves is affected significantly by the filler inclusion, leading to mastic with different behaviour. The parameter C refers to the integrity of the material, and it is assumed as 1.0 at the beginning of the test (materials without damage) and 0 (or nearly 0) at the end. The parameter D (damage intensity) indicates the quantity of work that is needed to make a decrease in the C parameter in the specimens.

Different mastics express different damage progression related to the resistance to fatigue damage. Based on the C-D curves, all fillers improve the damage resistance of the CBE binder. However, the LS mastic has an unfavourable damage curve compared to CBE binder as it accelerates the reduction of integrity (C). This could be attributed to the low reactivity of LS filler (inactive filler) within the CBE binder as described in Figure 5. While the SF mastic shows early rapid damage at the initial stage. However, the rest of the mastics show a steadier reduction in parameter C. This implies that they have the ability to sustain far more damage than the BE, SF, and LS. Taking GE mastic as an example, at a specific D value, it exhibited higher material integrity, indicating a better fatigue resistance. However, although ET mastic was stiffer than mastic GE, the loss in integrity was reached with lower damage amount. CE mastic exhibited a lower capability to withstand additional deformation levels that are recognized by the earlier reduction in shear stress after approaching the peak level (see Figure 11).

Consequently, the greater strain levels in CE mastic are counterpoised by a rapid decrease in the integrity parameter, leading to lesser damage intensity at the same C value. The curve trend for the brittle and stiff mastic (e.g., CE) is characteristically recognized by a higher peak of stress with a steep post-peak slope, signifying stiff fatigue failure. However, the damage evolution analysis cannot give or say the entire story regarding the fatigue resistance. Therefore, the fatigue power-law model was fitted to integrity-damage characteristics and utilized to obtain the fatigue laws and lives in order to compare the LAS results with other TS approaches as illustrated in Figure 14 and Table 5.

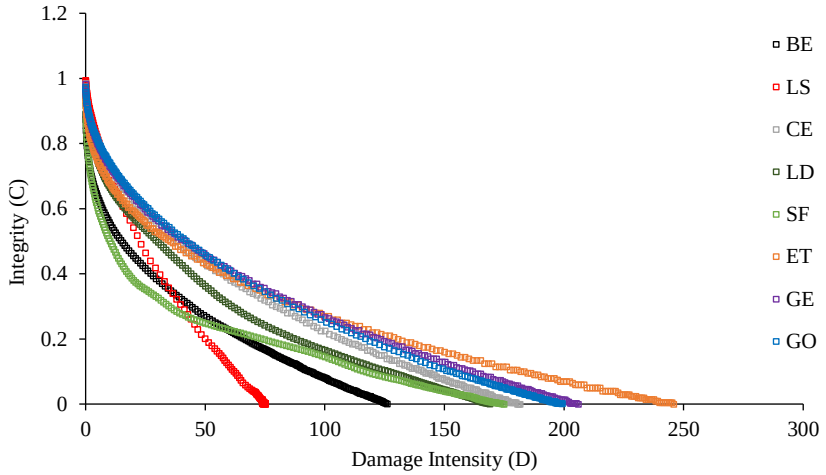

Figure 13. VECD Damage curve from amplitude sweep

3.3.3 Fatigue results comparison

Figure 14 and Table 5 show and compare the fatigue laws and lives, respectively, obtained from TS and LAS tests. Generally, the predicted fatigue resistance with time sweep test is longer than that of the LAS predictions, and that agreed with other researchers [49]. The exception was BE and LS mastic, which have similar performance in the LAS analysis. This is because the LAS test is based on an accelerated procedure; thus, the intensity of damage for the same C reduction is higher. Moreover, both tests are subjected to different effects (reversible phenomena) which are not taken into consideration in the study. As it is known, the TS test is influenced by nonlinearity and thixotropy, while only the nonlinearity for the LAS test. Therefore, they provide very different laws (see Figure

Preprints (www.preprints.org) | NOT PEER-REVIEWED | Posted: 13 September 2020 doi:10.20944/preprints202009.0278.v1

14). However, both lines offer comparable outcomes about filler impact. From Table 5, it can be observed that the fatigue life of CBE and all mastics decreased considerably as the strain increased. Despite there are slight differences between the fatigue laws for the same mastic, the ranking of mastics was the same for each approach (approaches used to analyses TS data). Besides, it was observed that the filler type has a strong effect on fatigue law. Generally, each filler led to a remarkable improvement of fatigue performance as compared to the CBE binder, knowing that the used fillers increase the complex shear modulus of CBE significantly, as illustrated in Figure 10. Commonly, in strain-controlled time sweep test, mastic with the higher complex shear modulus (due to solid particle reinforcement) presents lower fatigue resistance. The reason behind that is, larger particle to particle contact leads to greater complex shear modulus, which in turn, causes a rise in the stress levels and the mastic withstands a smaller amount of damage at failure (fragile response).

Table 5. The fatigue life of different mastics determined with different approaches

Sample	Strain Level (%)	Fatigue failure criteria					
		RDEC	$G_{50\%}$	DER	DPA	ESR	LAS
BE	1.5	5930	6325	6151	6142	5805	6766
	2.5	1810	1540	1612	1636	1827	1875
	3.5	828	608	668	684	853	805
LS	1.5	1738	2219	1634	1369	2093	4843
	2.5	781	1052	746	742	970	1234
	3.5	462	643	445	496	585	501
CE	1.5	14661	31745	23768	19978	31967	16704
	2.5	7124	8767	8007	7011	9658	4368
	3.5	4428	3756	3910	3517	4391	1806
LD	1.5	17347	21148	19847	22298	24098	11636
	2.5	5239	5757	5346	5739	6517	3087
	3.5	2381	2444	2253	2347	2754	1288
SF	1.5	36011	44432	39389	42515	51422	22413
	2.5	10434	11244	10778	10721	12900	2837
	3.5	4614	4548	4590	4326	5188	745
ET	1.5	143888	109384	131017	98243	147797	30629
	2.5	34599	30549	34893	30203	49106	6544
	3,5	13532	13186	14597	13888	23765	2368
GE	1.5	40124	50493	47179	42030	50728	23042
	2.5	15811	19287	18497	16767	31739	5857
	3.5	8562	10232	9983	9153	23305	2377
GO	1.5	53856	73435	55072	48932	63505	22439
	2.5	16719	18736	16673	14331	17502	5651
	3.5	7737	7620	7590	6382	7489	2278

Nonetheless, this effect is filler content dependent. In this regard, Liao et al. [50] found that the fatigue laws of mastics with diluted suspension have no dependency on the testing mode (controlled strain or stress) whereas the testing mode has an effect on the mastics with concentrated suspension. Recall, in this experimental work, low filler content was used in order to obtain dilute suspension mastics to eliminate the effect of the particle to particle contact phenomena. Furthermore, Little and Petersen [51] figured out that in a controlled strain mode, active fillers modified mastic (i.e., hydrated lime) with greater complex shear modulus, presented a higher fatigue resistance due to its higher ability to hold larger damage levels at failure than the neat binder. To come to the point, using active filler leads to increase in complex shear modulus and in the elastic behaviour as stated in viscoelastic analyses and this was not accompanied with a significant decrease in the ductility for specific filler.

BE SF GE ET LS CE LD GO

Preprints (www.preprints.org) | NOT PEER-REVIEWED | Posted: 13 September 2020 doi:10.20944/preprints202009.0278.v1

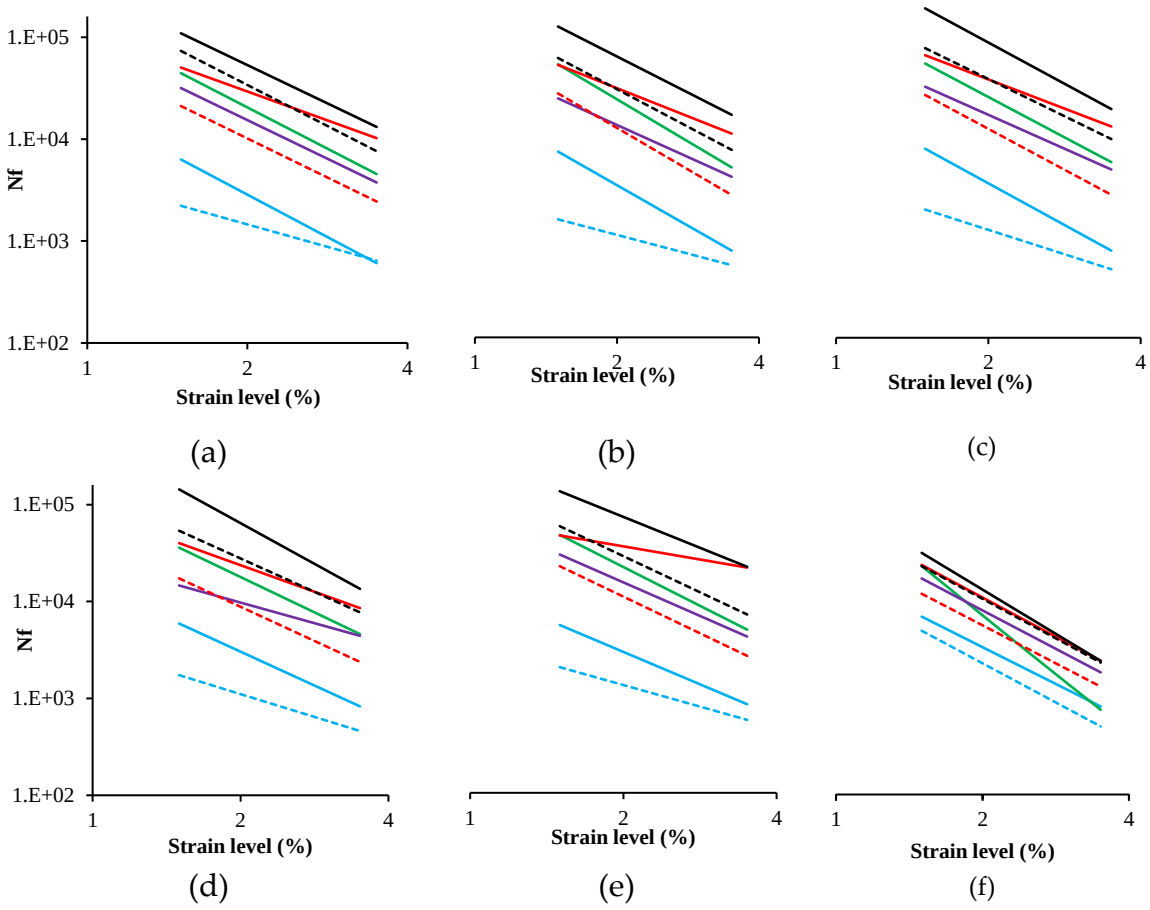

Figure 14. Fatigue laws derived from different failure approach: **(a)** $G_{50\%}$; **(b)** DPA; **(c)** DER; **(d)** RDEC; **(e)** ESR; **(f)** LAS 3.4 Physicochemical interaction of CBE mastic

As mention previously, fillers reinforce CBE mastic in three main mechanisms include volume filling (filler density), particle geometry, and chemical interaction. The first two mechanisms are considered as mechanical reinforcement. The last mechanism includes filler affinity to bitumen (basic or acidic nature) and the way at which it interacts with CBE binder (adhesion between the particle and bitumen; and hydraulic binder network). Regarding the volume filling effect, low filler content was used in this work in order to obtain dilute suspension mastics to eliminate the effect of the particle to particle contact phenomena. Therefore, filler reactivity is expected to dominant the CBE mastic performance. Table 6 shows that low-density filler, such as SF filler, increase the complex shear modulus and decrease the phase angle as more solid particles are added to the matrix (no expected reactivity effect as SF is low reactive filler when it is used alone in mastic) with moderate fatigue life.

On the contrary, a filler such as CE (high reactivity and density) leads to very stiff materials even with low particle concertation due to the formed rigid hydration products. This consequence can be clearly reflected in the fatigue resistance of CE mastic, as shown in Table 6. On the other hand, an inert filler such as LS, which also has relatively high density, exhibited lower complex shear modulus and higher phase angle with poor fatigue life. Normally, in the case of inert filler, the complex shear modulus comes from solid particle inclusion (no or little chemical reaction, see Figure 5). Thus, the low fatigue life is due to the poor reactivity of LS filler (poor affinity of LS particles to bitumen which weakened and divided the continuous phase of bitumen medium). However, this is not the case with active filler, as the hydraulic binder after the hydration process controls the rheological behaviour of the mastic matrix. Therefore, the expected improvement in fatigue resistance in this study mainly comes from chemical interaction. In this concern, filler chemistry could play a crucial role in affecting the fatigue life of mastic.

Preprints (www.preprints.org) | NOT PEER-REVIEWED | Posted: 13 September 2020 doi:10.20944/preprints202009.0278.v1

Table 6. Complex shear modulus, phase angle and filler density of corresponding mastics at 20°C temperature.

Sample	Complex shear modulus (Pa)	Phase angle (°)	Density (cm^3/g)	Fatigue ($G_{50\%}$)
BE	3.48E+06	57	-	1.54E+03
LS	2.78E+06	55	2.73	1.05E+03
CE	9.73E+06	54	3.14	8.77E+03
LD	3.37E+06	59	2.58	1.87E+04
SF	6.52E+06	48	2.27	1.12E+04
ET	1.04E+07	49	2.62	3.05E+04
GE	4.00E+06	56	2.45	1.93E+04
GO	6.00E+06	55	2.45	5.76E+03

Figure 15 shows a linear correlation between SO_3 content and corresponding mastic fatigue life. SO_3 rich filler (i.e. Gypsum) normally is incorporated for the purpose of regulating the setting time of hydration in cementitious binders. Tricalcium aluminate (C3A) is one of the main constituents of the cementitious binder; it can react with water strongly and lead to a rapid setting. Therefore, calcium sulphate such as Gypsum is generally added to cement to control C3A hydration. In the presence of calcium sulphate, a calcium sulfoaluminate compound, named ettringite is formed. The ettringite is very fine-grained crystals in shape that form a coating on the surface of the C3A particles. These crystals are not large enough for bridging the gaps between the particles of cement, but it might provide the bitumen matrix with a reinforcement network [52], [53]. From Figure 14, it can be noticed that as SO_3 content increases, the number of cycles at failure increases. For LD, CE, and ET, the C3A reaction is controlled by the SO_3 content, while for SF and GO, the situation is different. SF has no or tiny amount of CaO and SO_3 compounds, whereas GO contains a large amount of Fe_2O_3 (from FA filler) that could affect the fatigue life negatively. Besides, LS and GE fillers were not taken into account because LS is inert filler and does not have both earlier mention compounds while GE has the same GO chemical composition but with activator inclusion. From another perspective, a potential chemical interaction can be developed between the emulsifier and the carbonate anion, which comes from the active filler, forming salt at the interface zone. This salt can act as, at the interface, adhesion enhancer (increase the particle-bitumen affinity). That is why the cationic bitumen emulsion is favoured in CBE mixture [54]. Thus, an appropriate choice of filler with suitable emulsifiers, could act as a layer and use the water from the aggregate surface and help in good adhesion. In a nutshell, it can be concluded that fatigue resistance is correlated to more than one factor affecting simultaneously; balancing these factors is the key to enhancing and maintaining good fatigue damage resistance.

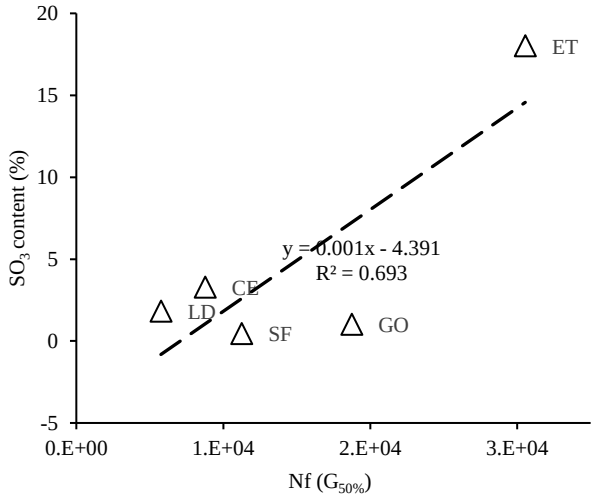

Figure 15. Correlation of fatigue life of CBE binder with SO_3 content (%)

4. Conclusions

In this study, the rheological characteristics and fatigue damage performance of CBE binder and mastics with different fillers were studied with the aid of chemical reactivity test (rise in pH test). The rheological response was represented by the master curve and modelled by the sigmoid model. Besides, fatigue damage performance was analyzed by time sweep tests (five approaches) and by linear amplitude sweep test. In this framework, the following findings can be drawn:

- Each active filler offered unique rheological behaviour and stiffening potential in terms of changing the LVE behaviour from that of viscous behaviour to that of viscoelastic behaviour.
- CBE mastics containing ladle slag fillers exhibited higher complex shear modulus at high temperatures. That might be due to a stable mastic matrix strengthened by the stiffness of LD particles, as well as the expected chemical action between alkaline components in LD fillers and water that is confirmed by chemical analyses test.
- The sigmoid model and the TTSP were successfully applied and statistically verified for describing the rheological performance of CBE mastics with excellent approximation.
- The fatigue resistance of the CBE binder is enhanced significantly by incorporating active fillers. However, the ET filler causes more improvement than that of the rest, bearing in mind that the used fillers increase the complex shear modulus of CBE significantly.
- The chemical analyses can be used effectively to identify the filler alkalinity and then estimate filler effect on mastic characteristics in the mixture.
- A good correlation between filler chemical composition (SO_3 content) and fatigue resistance was noticed. However, further investigation is required in this regard.
- The expected fatigue lives with time sweep test are generally longer than that of the LAS predictions. However, both testing procedures showed the same outcomes about the filler impact (similar ranking).
- For the time sweep test, all used approaches are all valid and offer comparable fatigue life results. However, the traditional approach ($G^*_{50\%}$) defines fatigue failure in an arbitrary way; thus, inaccurate analyses could have resulted.
- Despite the fact that the RDEC method has an interesting concept (focusing on the change in the dissipated energy), the experimental raw data, in some cases, difficult to recognize.
- The LAS test was successfully applied to CBE mixture and gave comparable results with a very short testing time (30 min). However, it depends on complex assumptions and procedures.
- Up to now, the role of active fillers on fatigue damage performance of CBE mastic was not well investigated, and there are only inadequate studies available on the topic. The findings from this research cast light on this vital subject

Funding: This research was funded by the German Academic Exchange Service (DAAD).

Conflicts of Interest: The authors declare no conflict of interest

References

1. M. I. Giani, G. Dotelli, N. Brandini, and L. Zampori, "Comparative life cycle assessment of asphalt pavements using reclaimed asphalt, warm mix technology and cold in-place recycling," *Resour. Conserv. Recycl.*, 2015.
2. J. Turk, A. Mauko Pranjić, A. Mladenovič, Z. Cotič, and P. Jurjavčič, "Environmental comparison of two alternative road pavement rehabilitation techniques: Cold-in-place-recycling versus traditional reconstruction," *J. Clean. Prod.*, 2016.
3. D. Lesueur, A. Teixeira, M. M. Lázaro, D. Andaluz, and A. Ruiz, "A simple test method in order to assess the effect of mineral fillers on bitumen ageing," *Constr. Build. Mater.*, 2016.

4. K. Z. Yan, H. Bin Xu, and H. L. Zhang, "Effect of mineral filler on properties of warm asphalt mastic containing Sasobit," *Constr. Build. Mater.*, 2013.
5. A. Al-Mohammedawi, K. Mollenhauer, "Viscoelastic Response of Bitumen Emulsion Mastic with Various Active Fillers," in *9th International Conference on Maintenance and Rehabilitation of Pavements and Technological Control, MAIREPAV 2020*, 2020.
6. P. Buczyński and M. Iwański, "Inactive Mineral Filler as a Stiffness Modulus Regulator in Foamed Bitumen-Modified Recycled Base Layers," in *IOP Conference Series: Materials Science and Engineering*, 2017.
7. V. B. Kakade, M. A. Reddy, and K. S. Reddy, "Rutting performance of hydrated lime modified bituminous mixes," *Constr. Build. Mater.*, 2018.
8. J. Temuujin, A. van Riessen, and R. Williams, "Influence of calcium compounds on the mechanical properties of fly ash geopolymer pastes," *J. Hazard. Mater.*, 2009.
9. D. Dutta, S. Thokchom, P. Ghosh, and S. Ghosh, "Effect of silica fume additions on porosity of fly ash geopolymers," *J. Eng. Appl. Sci.*, 2010.
10. M. Steveson and K. Sagoe-Crentsil, "Relationships between composition, structure and strength of inorganic polymers," *J. Mater. Sci.*, 2005.
11. M. Criado, W. Aperador, and I. Sobrados, "Microstructural and mechanical properties of alkali activated Colombian raw materials," *Materials (Basel).*, 2016.
12. S. C. Choi and W. K. Lee, "Effect of Fe2O3 on the physical property of geopolymer paste," in *Advanced Materials Research*, 2012.
13. C. Clopotel, R. Velasquez, and H. Bahia, "Measuring physico-chemical interaction in mastics using glass transition," in *Asphalt Paving Technology: Association of Asphalt Paving Technologists-Proceedings of the Technical Sessions*, 2012.
14. M. Kim and W. G. Buttlar, "Stiffening mechanisms of asphalt-aggregate mixtures: From binder to mixture," *Transp. Res. Rec.*, 2010.
15. B. S. Underwood and Y. R. Kim, "Experimental investigation into the multiscale behaviour of asphalt concrete," *Int. J. Pavement Eng.*, 2011.
16. P. J. Rigden, "The use of fillers in bituminous road surfacings. A study of filler-binder systems in relation to filler characteristics," *J. Soc. Chem. Ind.*, 1947.
17. A. F. Nikolaides, "Bituminous Mixtures & Pavements VI," in *Bituminous Mixtures and Pavements VI - Proceedings of the 6th International Conference on Bituminous Mixtures and Pavements, ICONFBMP 2015*, 2015.
18. X. Fang, A. Garcia-Hernandez, and P. Lura, "Overview on cold cement bitumen emulsion asphalt," *RILEM Tech. Lett.*, vol. 1, p. 116, 2016.
19. Q. Dai and M. H. Sadd, "Parametric model study of microstructure effects on damage behavior of asphalt samples," *Int. J. Pavement Eng.*, 2004.
20. D. A. Anderson and W. H. Goetz, "Mechanical behavior and reinforcement of mineral filler-asphalt mixtures," *J. Assoc. Asph. Paving Technol.*, vol. 42, pp. 37–66, Jan. 1973.
21. D. A. Anderson, J. P. Tarris, and J. D. Brock, "DUST COLLECTOR FINES AND THEIR INFLUENCE ON MIXTURE DESIGN.," in *Asphalt Paving Technology: Association of Asphalt Paving Technologists-Proceedings of the Technical Sessions*, 1982.
22. P. S. Kandhal, "EVALUATION OF BAGHOUSE FINES IN BITUMINOUS PAVING MIXTURES (WITH DISCUSSION)," vol. 50, 1981.
23. L. Ziyani, V. Gaudefroy, V. Ferber, D. Deneele, and F. Hammoum, "Chemical reactivity of mineral aggregates in aqueous solution: Relationship with bitumen emulsion breaking," *J. Mater. Sci.*, vol. 49, no. 6, pp. 2465–2476, 2014.
24. Z. Zizi, D. Oulahna, A. Benhassaine, A. Sainton, and M. Pelon, "'Emulsion - fine siliceous solids' system. The physical breaking of the emulsion," *Bull. des Lab. des Ponts Chaussees*, 1997.
25. C. Gaestel, "The breaking mechanism of cationic bitumen emulsions," *Chem. Ind.*, 1967.
26. R. Luo, D. Zhang, Z. Zeng, and R. L. Lytton, "Effect of surface tension on the measurement of surface energy components of asphalt binders using the Wilhelmy Plate Method," *Constr. Build. Mater.*, 2015.
27. A. Al-Mohammedawi and K. Mollenhauer, "A Study on The Fatigue Behavior Of Bitumen Emulsion Mastic, Modified with Various Active Fillers," in *Proceedings of the RILEM International Symposium on Bituminous Materials*, S. Di Benedetto, H., Baaj, H., Chailleux, E., Tebaldi, G., Sauzeat, C., Mangiafico, Ed. Lyon (France), 2020.

28. G. Mazzoni, A. Stimilli, F. Cardone, and F. Canestrari, "Fatigue, self-healing and thixotropy of bituminous mastics including aged modified bitumens and different filler contents," *Constr. Build. Mater.*, 2017.
29. M. Marasteanu, D. Ghosh, A. Cannone Falchetto, and M. Turos, "Testing protocol to obtain failure properties of asphalt binders at low temperature using creep compliance and stress-controlled strength test," *Road Mater. Pavement Des.*, vol. 18, no. 0, pp. 352–367, 2017.
30. A. A. Tayebali, G. M. Rowe, and J. B. Sousa, "Fatigue response of asphalt-aggregate mixtures," in *Asphalt Paving Technology: Association of Asphalt Paving Technologists-Proceedings of the Technical Sessions*, 1992.
31. A. C. Pronk, "Comparison of 2 and 4 point fatigue tests and healing in 4 point dynamic bending test based on the dissipated energy concept," *Eighth Int. Conf. Asph. Pavements*, 1997.
32. G. M. Rowe, "Application of the dissipated energy concept to fatigue cracking in asphalt pavements," 1996.
33. D. Mitchell, M. Witczak, M. Mamlouk, M. Kaloush, and K. Kaloush, "Validation Of Initial and Failure Stiffness Definitions in Flexure Fatigue Test for Hot Mix Asphalt," *J. Test. Eval.*, 2007.
34. Y. R. Kim, D. N. Little, and R. L. Lytton, "Fatigue and healing characterization of asphalt mixtures," *J. Mater. Civ. Eng.*, 2003.
35. H. Wen and H. Bahia, "Characterizing Fatigue of Asphalt Binders with Viscoelastic Continuum Damage Mechanics," *Transp. Res. Rec. J. Transp. Res. Board*, 2010.
36. H. Nguyen *et al.*, "Byproduct-based ettringite binder – A synergy between ladle slag and gypsum," *Constr. Build. Mater.*, vol. 197, pp. 143–151, 2019.
37. Y. R. Kim, *Modeling of Asphalt Concrete*. 2009.
38. A. T. Papagiannakis and E. A. Masad, *Pavement Design and Materials*. 2012.
39. G. D. Airey, B. Rahimzadeh, and A. C. Collop, "Viscoelastic linearity limits for bituminous materials," *Mater. Struct. Constr.*, vol. 36, no. 264, pp. 643–647, 2003.
40. C. Hintz, R. Velasquez, C. Johnson, and H. Bahia, "Modification and validation of linear amplitude sweep test for binder fatigue specification," *Transp. Res. Rec.*, 2011.
41. C. Johnson, "ESTIMATING ASPHALT BINDER FATIGUE RESISTANCE USING AN ACCELERATED TEST METHOD," University of Wisconsin – Madison, Madison, USA., 2010.
42. C. Johnson and H. Bahia, "Evaluation of an accelerated procedure for fatigue characterization of asphalt binders," *… Publ. Road Mater. …*, 2010.
43. R. A. Schapery, "Correspondence principles and a generalized J integral for large deformation and fracture analysis of viscoelastic media," *Int. J. Fract.*, 1984.
44. N. Tran and K. Hall, "Evaluating the predictive equation in determining dynamic moduli of typical asphalt mixtures used in Arkansas," 2005.
45. B. WU, D. S. van MAREN, and L. LI, "Predictability of sediment transport in the Yellow River using selected transport formulas," *Int. J. Sediment Res.*, 2008.
46. B. Wu, A. Molinas, and P. Y. Julien, "Bed-material load computations for nonuniform sediments," *J. Hydraul. Eng.*, 2004.
47. N. Tran and K. D. Hall, "Evaluating the predictive equation in determining dynamic moduli of typical asphalt mixtures used in Arkansas." 2005.
48. M. Češnovar, K. Traven, B. Horvat, and V. Ducman, "The potential of ladle slag and electric arc furnace slag use in Synthesizing alkali activated materials; the influence of curing on mechanical properties," *Materials (Basel).*, 2019.
49. I. S. Bessa, K. L. Vasconcelos, V. T. F. Castelo Branco, and L. L. B. Bernucci, "Fatigue resistance of asphalt binders and the correlation with asphalt mixture behaviour," *Road Mater. Pavement Des.*, vol. 20, no. sup2, pp. S695–S709, Jul. 2019.
50. M. C. Liao, J. S. Chen, and K. W. Tsou, "Fatigue characteristics of bitumen-filler mastics and asphalt mixtures," *J. Mater. Civ. Eng.*, 2012.
51. D. N. Little and J. C. Petersen, "Unique effects of hydrated lime filler on the performance-related properties of asphalt cements: Physical and chemical interactions revisited," *J. Mater. Civ. Eng.*, 2005.
52. P. K. MEHTA, "Morphology of Calcium Sulfoaluminate Hydrates," *J. Am. Ceram. Soc.*, 1969.
53. A. Quennoz, "Hydration of C3A with Calcium Sulfate Alone and in the Presence of Calcium Silicate," vol. 5035, pp. 8–10, 2011.
54. J. Sjoblom, "Emulsions and Emulsion Stability: Surfactant Science Series/61," *CRC Press*, 2005.